Bifurcation Analysis of Nose-Landing-Gear Shimmy with Lateral and Longitudinal Bending

Phanikrishna Thota,* Bernd Krauskopf,† and Mark Lowenberg‡
University of Bristol, Bristol, England BS8 1TR, United Kingdom

This work develops and studies a model of an aircraft nose landing gear with torsional, lateral, and longitudinal degrees of freedom. The corresponding three modes are coupled in a nonlinear fashion via the geometry of the landing gear in the presence of a nonzero rake angle, as well as via the nonlinear tire forces. Their interplay may lead to different types of shimmy oscillations as a function of the forward velocity and the vertical force on the landing gear. Methods from nonlinear dynamics, especially numerical continuation of equilibria and periodic solutions, are used to asses how the three modes contribute to different types of shimmy dynamics. In conclusion, the longitudinal mode does not actively participate in the nose-landing-gear dynamics over the entire range of forward velocity and vertical force.

Nomenclature

c_β	=	longitudinal bending damping of strut
c_δ	=	lateral bending damping of strut
c_λ	=	damping coefficient of elastic tire
c_ψ	=	torsional damping of strut
e	=	caster length
e_{eff}	=	effective caster length
F_{K_λ}	=	lateral tire force or cornering force
F_z	=	vertical load on the gear
h	=	contact patch length of elastic tire
I_x	=	moment of inertia of strut with regard to x axis
I_y	=	moment of inertia of strut with regard to y axis
I_z	=	moment of inertia of strut with regard to z axis
k_α	=	self-aligning coefficient of elastic tire
k_β	=	longitudinal bending stiffness of strut
k_δ	=	lateral bending stiffness of strut
k_λ	=	restoring coefficient of elastic tire
k_ψ	=	torsional stiffness of strut
L	=	relaxation length
l_g	=	gear height
M_{D_α}	=	moment due to tire lateral damping
M_{D_β}	=	moment due to damping in the longitudinal mode
M_{D_δ}	=	moment due to damping in the lateral bending mode
M_{D_ψ}	=	moment due to damping in the torsional mode
M_{K_α}	=	self-aligning moment due to tire force
M_{K_β}	=	moment due to stiffness in the longitudinal mode
M_{K_δ}	=	moment due to stiffness in the lateral bending mode
M_{K_ψ}	=	moment due to stiffness in the torsional mode
M_{λ_β}	=	coupling moment between the tire deformation and longitudinal mode
M_{λ_δ}	=	coupling moment between the tire deformation and lateral mode
R	=	radius of nose wheel
V	=	forward velocity of the aircraft
α_m	=	self-aligning moment limit
β	=	longitudinal bending angle
γ	=	wheel tilt or camber angle
δ	=	lateral bending angle
θ	=	swivel angle
ϕ	=	rake angle
ψ	=	torsion angle

I. Introduction

UNWANTED oscillations in wheeled vehicles, generally referred to as shimmy oscillations, can be caused by a variety of factors, such as component flexibilities, free play, etc. [1–4]. Even though the triggering mechanism for shimmy oscillations may vary in different types of vehicles, the consequences of such oscillations are wear and tear of components and discomfort to the riders. Specifically, in the case of aircraft landing gears considered here, extreme shimmy oscillations can result in high maintenance costs and also in violent vibrations in the cockpit [5,6], sometimes even restricting the pilot's ability to read the instrument panel.

Efforts to study shimmy oscillations, initially in cars, date back to the early 1900s. As entry points to the literature see, for example, the surveys by Dengler et al. [7], Smiley [8], and Pritchard [9], who discuss theoretical as well as experimental studies, stressing both tire theories and structural aspects of shimmy oscillations. Broulhiet's [10] seminal work on the effect of side slip of an elastic tire on shimmy oscillations forms the basis for many modern shimmy studies. However, it was von Schlippe and Dietrich [11] who developed one of the earliest and still widely used models, the *stretched string model* of tire kinematics, and used it for shimmy analysis of an aircraft landing gear. Smiley [8] studied shimmy oscillations in aircraft for three different landing gear structures and studied them by means of linear stability analysis. Furthermore, he provided a comprehensive comparison of different tire models. Even though one of the landing gears Smiley considered included a nonzero rake angle, its nonlinear and geometric effects were not considered in his analysis. More recently, Somieski [12] performed time domain analysis of a set of nonlinear ordinary differential equations representing a nose landing gear. He reported that shimmy oscillations appear (and disappear) via a Hopf bifurcation [13,14] and exist over a range of velocities of the aircraft. A different approach was taken by Woerner and Noel [15], who studied shimmy oscillations by frequency analysis. They described the main cause of shimmy oscillations as the energy transfer from the contact force between the tires and the ground to vibrational modes of the landing gear. In particular, Woerner and Noel studied the dependence of frequency on the swivel friction and forward velocity; this suggested

*Research Assistant, Department of Engineering Mathematics, Queens Building, University Walk. Member AIAA.
†Professor, Department of Engineering Mathematics, Queens Building, University Walk.
‡Head of Department, Department of Aerospace Engineering, Queens Building, University Walk. Senior Member AIAA.

that coupled motion may occur due to resonance phenomena when the forward velocity changes, a mechanism that may lead to high-amplitude shimmy oscillations.

This paper studies the onset and stability of shimmy oscillations in an aircraft nose landing gear in a free rolling scenario with emphasis on the influence of different vibrational modes on the landing gear dynamics. This work considers the main three vibrational modes of a generic midsize commercial passenger aircraft: the torsional mode corresponding to the rotation about the gear strut axis, the lateral bending mode that is representative of vibrations of the gear from left to right, and the longitudinal bending mode in the direction of straight-line travel of the aircraft. These modes of vibration are coupled via the geometry of the gear and via the force generated at the tire–ground contact. Their nonlinear interaction plays an important role in aircraft shimmy dynamics. Note that, as is also the case in the past research on shimmy oscillations, the vertical mode associated with the oleos (shock dampers) of the gear is not included as part of the model considered here. Namely, it is known from operational practice that the vertical dynamics is not the triggering mechanism for shimmy oscillations, certainly for smooth runways and taxiways as used today. The only earlier work that mentions the vertical mode in the context of shimmy analysis is the work by Dengler et. al. [7], who conclude that shimmy is generally independent of the vertical degree of freedom. Furthermore, our previous work [16] concluded that the vertical degree of freedom does not influence the nature of shimmy oscillations in a nose landing gear in our model.

Specifically, a seven-dimensional ordinary differential equation model for the torsional, lateral, and longitudinal modes and the tire force is developed and studied. In a first-order approximation, each vibrational mode is modeled as a single degree of freedom oscillator, which is coupled with the other modes via the gear geometry and the tire–ground contact. The elastic tire is modeled by a modified version of the stretched string model [11] that includes the effect of the lateral bending mode on the deformation of the tire. Importantly, the case of a nonzero rake angle of the gear, which has consequences for the coupling of the modes via nonlinear geometric effects, is considered.

The model presented here is an extension of a five-dimensional model that was developed previously [17], which does not include the longitudinal degree of freedom, but allows for the nonlinear interaction between the torsional and lateral modes in an aircraft nose landing gear. This made it possible to identify types of shimmy oscillations that are dominated either by the torsional mode, the lateral mode, or transient behavior featuring contributions from both. In the latter case, one may find quasi-periodic shimmy oscillations, which are characterized by two incommensurate frequencies [13,14]. We remark that stable quasi-periodic shimmy oscillations have been found by Pacejka [18] in the quite different setting of a pulled trailer with zero rake angle and negligible damping.

Typically, the fundamental frequency of the longitudinal mode of a landing gear is in about the same range as that of the torsional and lateral bending modes. Moreover, the longitudinal mode is coupled to the other modes via the geometry of the gear and also the restoring force generated at the tire–ground contact. This coupling is nonlinear in nature, given the characteristics of the tire force and also due to the nonzero rake angle. In fact, due to the nonlinear nature of the problem, even small longitudinal motion might result in shimmy oscillations. Hence, it is a priori entirely possible that the longitudinal mode may be involved in shimmy oscillations. The main question that is addressed here is whether the inclusion of the longitudinal mode affects the dynamics in a significant way. To answer this question, we perform time and frequency domain analyses of the different types of shimmy oscillations with MATLAB®, in conjunction with a numerical bifurcation analysis with the software package AUTO [19]. This allows us to assess the role of the longitudinal mode over the entire relevant operational range of forward velocity of the aircraft and vertical force on the gear by means of one- and two-parameter bifurcation diagrams. This work also investigates how regions of different types of shimmy oscillations in the two-parameter bifurcation diagrams change with the damping in the torsional mode.

The paper is organized as follows. Section II introduces and discusses the mathematical model of the nose landing gear. Section III is devoted to the analysis of the model, in which we show representative time series and frequency spectra, one-parameter continuations in the forward velocity, and a two-parameter bifurcation diagram in the plane of forward velocity and vertical force on the gear. Section IV investigates the influence of torsional damping on the bifurcation diagrams. Finally, Sec. V summarizes and discusses directions of future research.

II. Model of a Nose Landing Gear

The nose landing gear of an aircraft as considered here is shown in Fig. 1. A wheel with a pneumatic tire of radius R is mounted on an axle that is connected to a strut via a mechanical caster (trail) of length e. The landing gear experiences a vertical load F_z while moving with a forward velocity V. The load F_z includes not only the static weight of the remainder of the aircraft but also the moments exerted on the gear due to its acceleration and deceleration. This modeling practice is also used in the literature [2,20]. Moreover, during testing of an aircraft, F_z is measured as one of the main parameters. Therefore, in our study F_z is used as an input and natural bifurcation parameter. One of the conventionally accepted coordinate systems for aircraft analysis is used, in which the positive x axis is along the fuselage centerline and points in the backward direction of the aircraft, the z axis is the upward normal to the flat ground, and the y axis completes the right-handed coordinate system. In the static equilibrium position of the gear, the strut axis lies in the (x, z) plane, and it is inclined to the vertical at a rake angle ϕ. Note that the rake angle varies significantly from one aircraft type to the other and may be anywhere in the range of 0–30 deg, whereas a range of 0–15 deg is more typical for commercial passenger aircraft.

Here, a nose landing gear with three geometrical degrees of freedom is considered. First, the gear may rotate about the strut axis S, which gives rise to the *torsional mode* described by the torsion angle ψ (rad). Second, the gear may bend about the x axis, which gives rise to the *lateral mode*. It is described in a first-order approach by the angle δ (rad) over which the strut is rotated about the mount point in the lateral direction. Third, the gear may bend about the y axis, which gives rise to the *longitudinal mode* as described by the angle β (rad) over which the strut is rotated in the longitudinal direction. The model considered here is an extension of the nose-landing-gear model presented in Thota et al. [17]. Specifically, the extra degree of freedom corresponding to the longitudinal motion as described by β is added to investigate its influence on the overall dynamics.
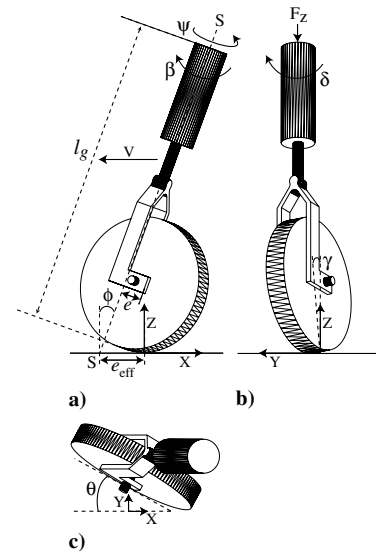

Fig. 1 Schematic views of an aircraft nose landing gear: a) side, b) front, and c) top.

where l_g is the distance between the point of attachment of the gear to the fuselage and the ground. The last term in Eq. (5) represents a destabilizing moment that is proportional to the vertical load on the aircraft. This moment becomes active in a significant way during landing of an aircraft, when there is a sudden increase in the vertical load.

Similarly, in Eq. (6) the coupling moment M_{λ_β} is given by

$$M_{\lambda_\beta} = l_g F_{K_\lambda} \sin(\theta)\cos(\phi + \beta) \qquad (13)$$

Again, the last term in Eq. (6) represents a destabilizing moment proportional to the vertical force F_z as well as to the sine of the effective rake angle. For a nonzero rake angle ϕ of the landing gear, this moment is responsible for a nonzero stable equilibrium position. This is different from the case in which the longitudinal degree of freedom β is not considered in the model, so that the equilibrium position is at zero [17].

C. Tire Kinematics

Equation (7) describes the motion of the tire under the influence of the strut's torsional, lateral, and longitudinal motions. Here, the resultant tire deformation is an algebraic sum of the deformation caused by the torsional and lateral modes. The effect of the lateral deformation caused due to the lateral bending mode [17] is incorporated into Eq. (7) by adding an extra term to the conventional equation representing the stretched string model [11]. Superimposing the effects of both the modes is justified by derivations that are not presented here. The longitudinal mode variable β enters into the tire motion via the effective caster length e_{eff} and the effective rake angle.

III. Nonlinear Dynamics of the Nose Landing Gear

We now consider the nonlinear dynamics of the mathematical model (4–7) of the nose landing gear. In Table 1, we summarize the values for the parameters used in this work, which are realistic choices for a generic midsized passenger aircraft that have been adapted from the literature [12,17] and complemented by data from Airbus internal reports. First, a time and frequency domain analysis of the model with MATLAB is presented for three different settings of the forward velocity V and the downward force F_z, which correspond to three different kinds of shimmy oscillations. This allows us to investigate the relative contributions of the three vibrational modes to the overall landing gear dynamics. Next, a one-parameter bifurcation study in the forward velocity V is presented to determine the relative strengths of the three modes over a larger range of operating conditions. Finally, a direct comparison of two-parameter bifurcation diagrams in the (V, F_z) plane of Eqs. (4–7) with and without an active longitudinal bending mode is presented. The bifurcation studies were performed with the numerical continuation package AUTO [22], which allows one to follow equilibria and periodic solutions and their bifurcations in system parameters.

A. Time and Frequency Domain Analysis

For the parameter values in Table 1, the linear damped natural frequencies of the torsional, lateral, and longitudinal modes in the case of an unloaded gear are 8.71, 11.69, and 50.32 Hz, respectively. These frequencies of the uncoupled linear modes are in realistic ranges for a midsize passenger aircraft. Because of the nonlinearities of the model, the frequencies of the three modes during shimmy oscillations will deviate somewhat from their natural frequencies, but they remain clearly distinguishable.

The lateral and longitudinal bending modes manifest themselves at the tire–ground interface as motions that deform the tire. Therefore, it is convenient to consider not the angular variables δ and β themselves, but their *strokes* at ground level as given by

$$\delta^* = l_g \sin(\delta) \quad \text{and} \quad \beta^* = l_g \sin(\beta) \qquad (14)$$

where l_g is the height of the gear. The strokes δ^* and β^* allow for a direct comparison of the amplitudes of the lateral and longitudinal motions relative to the tire deformation λ (measured in meters). Because all modes interact via the tire, the respective frequency components in the power spectrum of λ reveal the contributions of the three modes to the dynamics. To assess the role of the longitudinal bending oscillations, the power spectrum of β^* is considered as well.

Figures 2–4 show time histories and frequency spectra for three different sets of values of the velocity V and the vertical force F_z. Each figure illustrates the relative contributions of the different modes to different kinds of shimmy oscillations. In each figure, three time series panels (left column) show oscillations of the torsion angle ψ, of the tire deformation λ in comparison with the lateral stroke δ^*, and of the longitudinal stroke β^*, respectively. Notice the difference in scale, which shows that the longitudinal stroke β^* oscillates with negligible amplitudes, whereas the lateral stroke δ^* oscillates with amplitudes of several centimeters. The two spectra panels (right
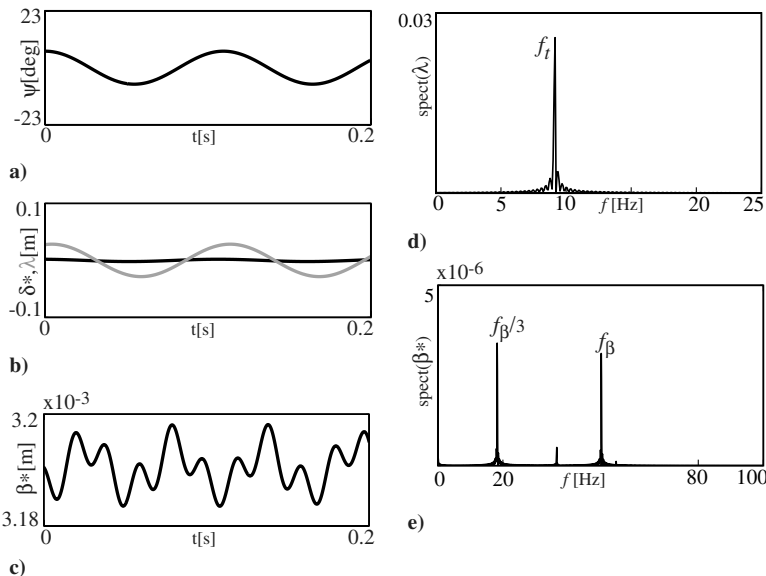
Fig. 2 $V = 20$ m/s and $F_z = 60$ kN: a), b), and c) time histories; and d) and e) frequency spectra. The individual panels show time series of the following: a) torsional mode variable, b) lateral stroke (black) and the tire deformation (gray), c) longitudinal stroke, and spectra of d) tire deformation, and e) the longitudinal stroke (where f_t, f_l, and f indicate the frequencies of the torsional, lateral, and longitudinal modes).

column) show the frequency content of the tire deformation λ and of the longitudinal stroke β^*.

Figures 2a–2e show shimmy oscillations for $V = 20$ m/s and $F_z = 60$ kN, a relatively low velocity and low vertical force. This type of shimmy dynamics can be identified as pure torsional shimmy: ψ oscillates with a considerable amplitude of about 7 deg, and this induces oscillations of the tire deformation λ (Figs. 2a and 2b) at the frequency $f_t \approx 8.79$ Hz of the torsional mode (Fig. 2d). The lateral mode is effectively following this excitation with a very small amplitude. However, the longitudinal mode is oscillating at the frequency $f_\beta \approx 49.8$ and $\frac{f_\beta}{3} \approx 16.6$ Hz, and with negligible amplitudes. Even though the stiffness in the longitudinal mode is slightly higher than in the lateral and torsional mode, the restoring effect of the coupling term M_{λ_β} extracts most of the energy out of the longitudinal mode.

For the higher-vertical-force case of $V = 5$ m/s and $F_z = 162$ kN in Figs. 3a–3e, a very different type of shimmy oscillations is found: pure lateral shimmy driving the torsional mode. Here, the lateral mode drives the tire deformation at a comparable amplitude of about 5 cm (Figs. 3b and 3d) and at a frequency $f_l \approx 11.72$ Hz. In contrast to the earlier case, the torsional mode follows this excitation by the lateral mode. Here, the longitudinal mode is oscillating at the frequency of the lateral motion $f_l \approx 11.7$ and $2f_l \approx 23.4$ but has no influence on shimmy oscillations.

A qualitatively different type of shimmy dynamics can be seen in Figs. 4a–4e for $V = 12$ m/s and $F_z = 162$ kN, in which an interaction between the torsional mode and the lateral bending mode is seen. In Figs. 4a and 4b, the modulation in the amplitudes of the torsional and lateral bending modes indicates an interplay of two *incommensurate* frequencies. The frequency spectrum given in Fig. 4d clearly shows that these two frequencies correspond to the torsional (f_t) and lateral bending (f_l) modes. The time histories shown in these panels correspond to a transient quasi-periodic behavior in the vicinity of a torus bifurcation [13,14]. Depending on the distance from the torus bifurcation, the transient behavior may last anywhere from tens to hundreds of seconds. In a situation such as takeoff or landing, during which the velocities change quite rapidly, such transient behavior plays an important role in the observed dynamics.

An important conclusion from Figs. 2–4 is that the longitudinal mode does not appear to contribute to the landing gear dynamics. Even though we considered three qualitatively different types of shimmy oscillations, the longitudinal mode is excited only very weakly, oscillates with a negligible amplitude, and does not influence either the torsional or the lateral mode.

B. Shimmy Oscillations as a Function of Forward Velocity V

This section investigates the role of the longitudinal bending mode for the nose gear dynamics as described by Eqs. (4–7) over the range of 0–110 m/s of the forward velocity V for two fixed values of the downward force F_z. Specifically, we perform a numerical continuation study of the equilibrium and bifurcating shimmy oscillations and their stability for the light and the heavy cases $F_z = 60$ and 162 kN. Note that this choice of F_z means that the examples of shimmy oscillations shown in Figs. 2–4 are covered by the one-parameter bifurcation diagrams presented here.

Figure 5 shows the resulting branches of solutions of two continuation runs in V for $F_z = 60$ and 162 kN. For each case, three panels show the maximum amplitude of the torsion angle ψ, of the lateral stroke δ^*, and of the longitudinal stroke β^*, respectively. Notice again the difference in scale between δ^* and β^*. The equilibrium solution of the gear, which corresponds to the desired straight-line motion, is represented by the straight line with zero amplitude in the panels. In both cases, a single branch of shimmy oscillations with nonzero amplitudes of the modes is found. The equilibrium and the shimmy oscillations may be stable (solid curves) or unstable (dashed curves). Note that the straight-line motion may be stable for low and high velocities V for a given range of downward force F_z. Stability changes at bifurcation points, such as the Hopf bifurcation at which the shimmy oscillations are born. Changes of stability at torus bifurcations of shimmy oscillations are also found; this means that a second frequency becomes involved in the gear motion.

Figures 5a, 5c, and 5e show a low-loading case for $F_z = 60$ kN. Here, even though the straight-line equilibrium is unstable for very low velocities, it becomes stable in a Hopf bifurcation corresponding to the lateral mode and remains stable for the velocity range of 2–9 m/s. As the velocity increases further, the stability of the stable equilibrium is lost in a Hopf bifurcation H at $V \approx 9.8$ m/s. This Hopf bifurcation is supercritical, and it gives rise to stable periodic shimmy oscillations. The relative maximal amplitudes show that this type of shimmy oscillation is dominated by the torsional mode. Its maximal amplitude initially grows with V but decreases again above $V \approx 20$ m/s (Fig. 5a). The lateral frequency effectively remains dormant (Fig. 5c) and the longitudinal motion is relatively small (Fig. 5e), which indeed agrees with the dynamics in Figs. 2a–2e. The branch of stable torsional shimmy oscillations reduces to zero amplitude at $V \approx 55.8$ m/s in a third Hopf bifurcation H. Beyond this bifurcation point, the straight-line equilibrium is stable and shimmy oscillations are not observed.
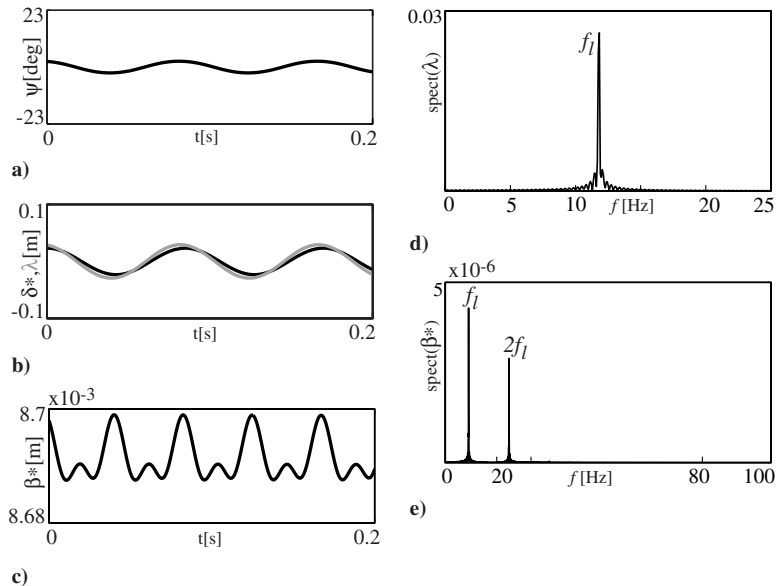

Fig. 3 $V = 5$ m/s and $F_z = 162$ kN: a), b), and c) time histories; and d) and e) frequency spectra.
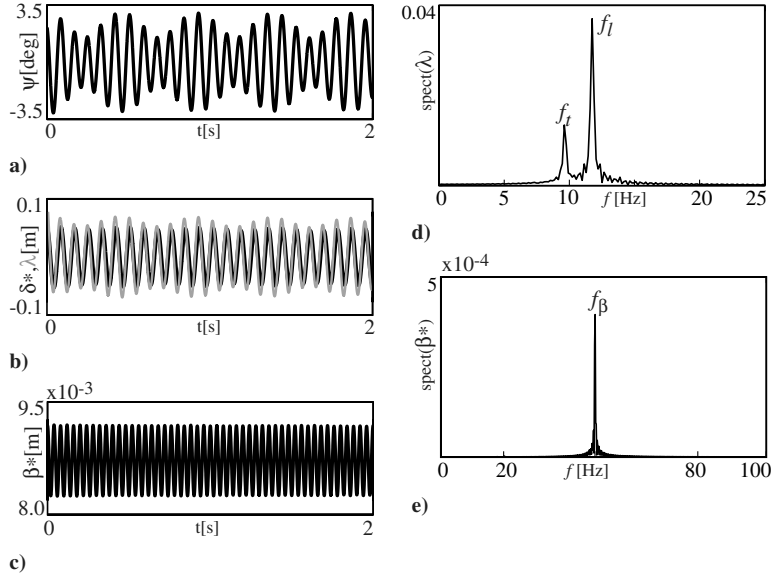
Fig. 4 $V = 12$ m/s and $F_z = 162$ kN: a), b), and c) time histories; and d) and e) frequency spectra.
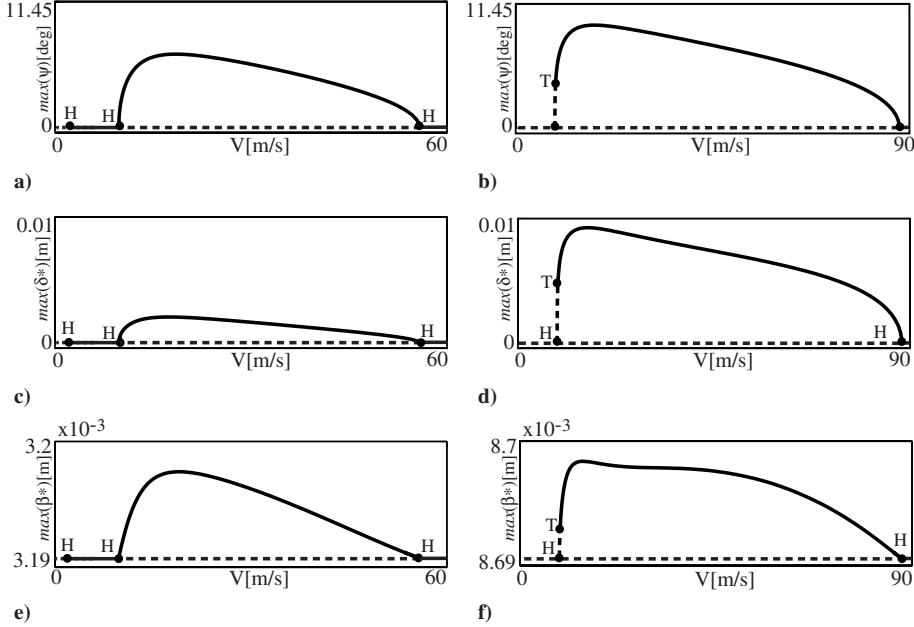

Fig. 5   One-parameter continuation in V: a), c), and e) $F_z = 60.0$ kN; and b), d), and f) $F_z = 162.0$ kN. The individual panels show the following: a) and b) maximum of the torsion angle ψ, c) and d) maximum of the lateral bending stroke δ^*, and e) and f) maximum of the longitudinal bending stroke β^*. The stable parts of branches are drawn as solid curves, whereas the unstable parts are dashed, with Hopf bifurcations labeled H and torus bifurcations labeled T.

Figures 5b, 5d, and 5f show some marked differences for the higher-loading case of $F_z = 162$ kN. Again, the straight-line equilibrium, which is already unstable, undergoes a stability change via a supercritical Hopf bifurcation H, now at $V \approx 9.2$ m/s. However, now the unstable shimmy oscillation that is born at the Hopf bifurcation quickly changes stability in a torus bifurcation T, which results in stable shimmy oscillations dominated by the torsional mode. The maximal amplitudes of the shimmy oscillations initially grow with V but then decrease again. Notice that the maximum amplitude of the torsional mode is now about 10 deg. It is reached around $V \approx 16$ m/s, after which it decreases substantially (Fig. 5b); this is mirrored on a much smaller scale by the longitudinal mode (Fig. 5f). The maximum amplitude of the lateral mode of about 10 cm is also attained at $V \approx 16$ m/s (Fig. 5d). The branch of stable shimmy oscillations disappears at $V \approx 88.2$ m/s in a second Hopf bifurcation H. We remark that in the unstable region before the torus

bifurcation the system jumps to stable pure lateral shimmy oscillations as shown in Figs. 3a–3e.

One of the main features of the one-parameter bifurcation diagrams in Fig. 5 is the negligible size of the longitudinal oscillations. Throughout the entire V range, and for both loading cases, the longitudinal stroke β^* is at least two orders of magnitude smaller than the lateral stroke, never exceeding 0.1 mm. This forms evidence that the longitudinal motion β is insignificant for the landing gear dynamics for a free-rolling nose landing gear.

C.   Bifurcation Diagram in the (V, F_z) Plane

The role of the longitudinal mode for the dynamics of the nose landing gear over the entire relevant range of the two main operational parameters V and F_z is considered here. To this end, Fig. 6 shows the two-parameter bifurcation diagram in the (V, F_z) plane of

the seven-dimensional Eqs. (4–7) and of the five-dimensional model where $\beta \equiv 0$, both computed with the package AUTO for the parameter values in Table 1.

Figure 6a is the two-parameter bifurcation diagram for the seven-dimensional model (4–7), which includes the longitudinal degree of freedom β. It provides a global summary of the dynamics of this model by presenting the locations of the main bifurcations. Specifically, the locations of Hopf bifurcations, saddle-node bifurcations, and torus bifurcations are shown. Along the curve H_t, one finds Hopf bifurcations of the torsional mode, meaning that the bifurcating shimmy oscillations are dominated by the torsional component. The curve H_t forms an isola (closed curve); the solid part of the curve H_t corresponds to supercritical Hopf bifurcations in which stable shimmy oscillations are born if the equilibrium before the bifurcation is stable, whereas the dashed part of H_t corresponds to subcritical Hopf bifurcations in which unstable shimmy oscillations bifurcate. The transition between the super- and subcritical parts of H_t occurs at two special points that are known as degenerate Hopf (DH) points [13,14]. Each of these DH points is the starting point of a curve of saddle-node (SN) bifurcations. There is also a curve H_l of Hopf bifurcations of the lateral bending mode. It intersects the torsional Hopf curve H_t in two points that are known as double-Hopf (HH) points. As predicted by bifurcation theory [13,14], we find that, locally, two curves of torus bifurcations emanate from each of the HH points. There are two main torus curves in Fig. 6a: along T_t one finds torus bifurcations of the torsional shimmy oscillations born at H_t, and along T_l one finds torus bifurcations of the lateral shimmy oscillations born at H_l. Note that the curves T_l and T_t both connect the two HH points.

Overall, the bifurcation curves in Fig. 6a organize the (V, F_z) plane into regions with different types of dynamics. The shaded region represents parameter values for which the straight-line equilibrium is stable, that is, there are no shimmy oscillations. Different regions bounded by the bifurcation curves correspond to different types of dynamics. Specifically, the three different types (a–c) of shimmy oscillations from Figs. 2–4 can be identified in Fig. 6a. In the region including (a), the torsional mode is dominant; in the region including (b), shimmy oscillations are dominated by the lateral mode; and in the region including (c), one may observe coupling between the torsional and lateral modes. Note further that the one-parameter bifurcation diagrams in Fig. 5 correspond to horizontal cross sections of Fig. 6a at $F_z = 60$ and 162 kN, respectively. The different bifurcations that are encountered as the forward velocity V is changed are readily identified.

Figure 6b shows the two-parameter bifurcation diagram for the five-dimensional model without inclusion of the longitudinal degree of freedom β. The agreement with the bifurcation diagram in Fig. 6a is immediate. The corresponding bifurcation curves differ by less than 1% across the entire (V, F_z) plane. The only minor difference between Figs. 6a and 6b is the fact that the isola of H_t encloses a slightly smaller area of the (V, F_z) plane in Fig. 6a. This is due to the

increase in the effective rake angle $(\phi + \beta)$ in the presence of the longitudinal mode β. Overall, the excellent agreement of the two bifurcation diagrams constitutes conclusive evidence over the entire range of the operating parameters V and F_z that the longitudinal motion β does indeed not influence the landing gear dynamics in any significant way.

IV. Effects of Torsional Damping

Now, a study of how the torsional damping c_ψ influences the bifurcation diagram in the (V, F_z) plane is performed. Here, the fact that the longitudinal mode β does not play a significant role in the dynamics of the landing gear is used, so that it suffices to consider the five-dimensional model where $\beta \equiv 0$. The damping c_ψ models the overall damping characteristics in the torsional mode of the nose landing gear. Specifically, it includes the damping associated with an extra torsional or shimmy damper that is often installed on landing gears to curtail torsional oscillations. The disadvantage of shimmy dampers is that they increase the mass of the landing gear, contributing to the overall weight of the aircraft. Hence, a study of the effects of torsional damping on shimmy oscillations is important for the evaluation and design of a landing gear.

Figure 7 shows two-parameter bifurcation diagrams for the torsional damping values $c_\psi = 150$ Nms rad^{-1} (Fig. 7a) and $c_\psi = 70$ Nms rad^{-1} (Fig. 7b), where all other parameters are as shown in Table 1. The two panels of Fig. 7 correspond to larger and smaller values of c_ψ than that of 110 Nms rad^{-1} given in Table 1 and used in Fig. 6. It is quite evident from Figs. 7a and 7b that, as torsional damping decreases, the torsional shimmy region enclosed by the curve H_t becomes significantly larger. In contrast, decreasing c_ψ reduces the region corresponding to lateral shimmy, but this is a small effect. This reduction is due to the transfer of energy from the lateral bending mode into the torsional mode.

We now investigate how the region (the isola) corresponding to torsional oscillations varies over a wider range of c_ψ values. To this end, Fig. 8 shows the minimum and maximum of the velocity along H_t as a function of c_ψ. The corresponding values H_t^{min} and H_t^{max} were computed for the seven different values of c_ψ that are marked as dots in Fig. 8. These data were then used to obtain the solid curves by spline interpolation. Torsional shimmy oscillations can occur in the shaded region bounded by the two interpolated curves. It is observed that, although a change in c_ψ has very little effect on H_t^{min}, it has a large effect on H_t^{max}. Specifically, for $c_\psi = 200$ Nms rad^{-1}, torsional oscillations can occur only between $V \approx 11$ and 50 m/s. At a lower value of c_ψ, say $c_\psi = 100$ Nms rad^{-1}, on the other hand, torsional oscillations are born above $V \approx 7$ m/s and may be sustained for velocities greater than the average takeoff velocity of a midsize passenger aircraft. As an extreme case, H_t^{min} and H_t^{max} for $c_\psi = 10$ Nms rad^{-1} are also calculated, where H_t^{max} is at $V \approx 1207$ m/s, which falls well outside the range of Fig. 8. A study in Thota et al. [17] found that H_t^{min} and H_t^{max} depend linearly on the rake angle ϕ.

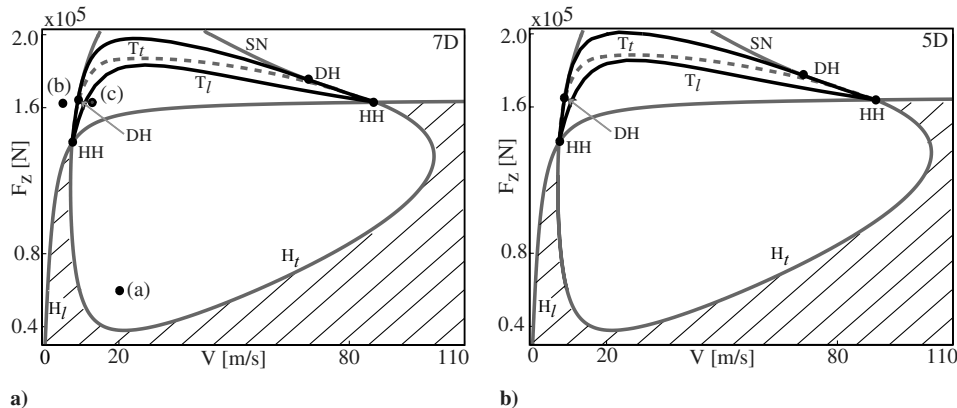a)   b)

Fig. 6   Two-parameter bifurcation diagram in the (V, F_z) plane of Eqs. (4–7) consisting of curves of Hopf bifurcations, saddle-node of limit cycle bifurcations, and torus bifurcations: a) longitudinal bending mode is active, and b) $\beta \equiv 0$, that is, without longitudinal bending.
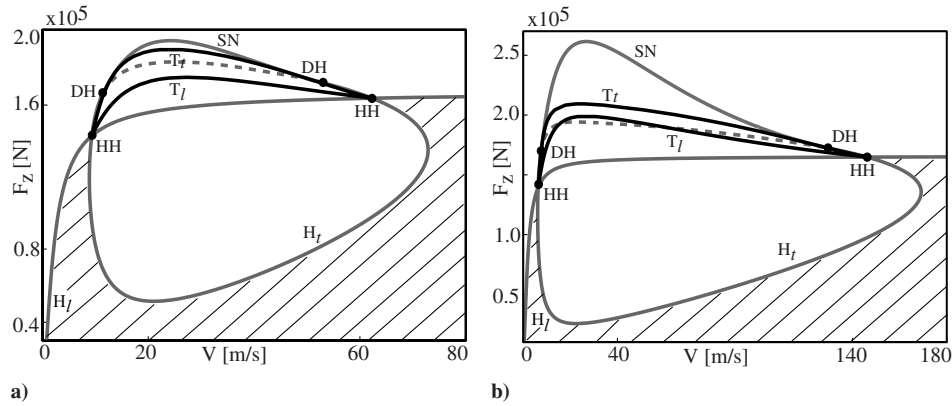
Fig. 7 Two-parameter bifurcation diagrams of Eqs. (4–7) in the (V, F_z) plane with parameter values as in Fig. 6b: a) $c_\psi = 150$ Nms rad^{-1}, and b) $c_\psi = 70$ Nms rad^{-1}.

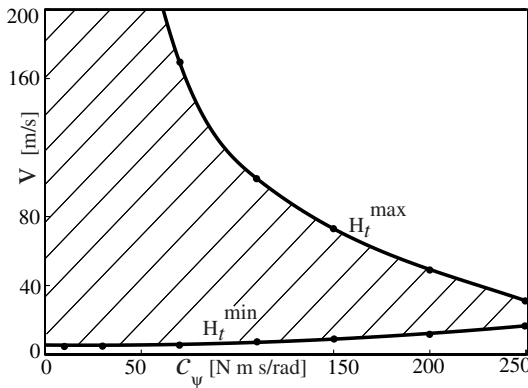**Fig. 8 The left-most point $H_t^{\min}$ and the right-most point $H_t^{\max}$ of the Hopf bifurcation curve H_t as a function of c_ψ. The shaded region corresponds to the area in the two-parameter bifurcation diagrams where torsional oscillations can occur.**

Such studies expand the existing knowledge of the parameter dependence of shimmy oscillations. In particular, they provide crucial sensitivity information that can assist in choosing optimal damping parameters over an entire operational range.

V. Conclusions

This work focused on the interaction of different vibrational modes in shimmy oscillations of the nose landing gear of a generic midsized passenger aircraft. Specifically, a seven-dimensional model that includes torsional, lateral, and longitudinal degrees of freedom was developed. Time histories and frequency spectra, in conjunction with a numerical bifurcation analysis in the forward velocity and the vertical force on the gear, showed that the torsional and the lateral bending modes interact very strongly to give rise to different types of shimmy oscillations. By contrast, the longitudinal degree of freedom does not actively participate in any of the different possible types of shimmy oscillations.

The overall conclusion is that the longitudinal degree of freedom can safely be omitted in the analysis of nose-landing-gear shimmy. Hence, without a sacrifice in qualitative and quantitative accuracy, it is sufficient to work with a five-dimensional model. This reduction in dimensionality and complexity of the model is of practical interest because it allows for more extensive bifurcation studies of the landing gear system. In this way, even quite complicated dynamical scenarios can be investigated. As an example, the investigation of the dependence of shimmy oscillations on torsional damping c_ψ was presented. The analysis concluded that the choice of appropriate overall torsional damping is crucial in minimizing the velocity range in which torsional shimmy occurs. In the longer term, dynamical scenarios, including acceleration during takeoff and braking after

landing, could be considered. In this case, forward velocity and vertical force are not independent of each other and their relationship can be derived from flight-test data. Furthermore, the study of a braking aircraft may require the inclusion of a vertical degree of freedom due to possible excitement of oleo (shock damper) dynamics. It would also be interesting to study the influence of other degrees of freedom on shimmy dynamics, in particular the torsional and lateral bending modes of the aircraft fuselage for the case of a larger passenger aircraft.

References

[1] Baumann, J., "A Nonlinear Model for Landing Gear Shimmy with Applications to the McDonnell Douglas G/A-18A," AGARD R-800, 1995.

[2] Besselink, I. J. M., "Shimmy of Aircraft Main Landing Gears," Ph.D. Dissertation, Univ. of Delft, The Netherlands, 2000.

[3] Glaser, J., and Hrycko, G., "Landing Gear Shimmy—De Havilland's Experience," AGARD R-800, 1995.

[4] Krabacher, W. E., "A Review of Aircraft Landing Gear Dynamics," AGARD R-800, 1995.

[5] Ligum. T. I., Skripnichenko. S. Yu., and Shishmarev. A. V., "Aerodynamics of Tu-154B Aircraft [in Russian]," Transport, Moscow, 1985.

[6] Plakhtienko. N. P., and Shifrin. B. M., "Critical Shimmy Speed of Nonswiveling Landing-Gear Wheels Subject to Lateral Loading," *International Applied Mechanics*, Vol. 42, No. 9, 2006.

[7] Dengler, M., Goland, M., and Herrman, G., "A Bibliographic Survey of Automobile and Aircraft Wheel Shimmy," Midwest Research Inst., Technical Rept. 52-141, Kansas City, MO, 1951.

[8] Smiley, R. F., "Correlation, Evaluation, and Extension of Linearized Theories for Tyre Motion and Wheel Shimmy," NACA 1299, 1957.

[9] Pritchard, I. J., "An Overview of Landing Gear Dynamics," NASA TM-1999-209143, 1999.

[10] Broulhiet, M. G., "La Suspension de la Direction de la Voiture Automobile—Shimmy et Dandinement," *Bulletin de la Societé áIngénierie Civile*, Vol. 78, 1925.

[11] Von Schlippe, B., and Dietrich, R., "Shimmying of a Pneumatic Wheel," NACA TM 1365, 1947.

[12] Somieski, G., "Shimmy Analysis of a Simple Aircraft Nose Landing Gear Model Using Different Mathematical Methods," *Aerospace Science and Technology*, Vol. 1, No. 8, 1997, 1270–9638.

[13] Guckenheimer, J., and Holmes, P., *Nonlinear Oscillations, Dynamical Systems and Bifurcations of Vector Fields*, Springer, New York, 1983, Chap. 6.

[14] Kuznetsov, Yu. A., *Elements of Applied Bifurcation Theory*, Springer, New York, 1995, Chap. 7.

[15] Woerner, P., and Noel, O., "Influence of Nonlinearity on the Shimmy Behaviour of Landing Gear," AGARD R-800, 1995.

[16] Krauskopf, B., Thota, P., and Lowenberg, M., "Geometric

Nonlinearities of Aircraft Systems," *Proceedings of ECMI 2008*, Institute of Mathematics and Its Applications, London, 2008.

[17] Thota, P., Krauskopf, B., and Lowenberg, M., "Interaction of Torsion and Lateral Bending in Aircraft Nose Landing Gear Shimmy," *Nonlinear Dynamics*, Vol. 57, 2009, pp. 455–467.
doi:10.1007/s11071-008-9455-y

[18] Pacejka, H. B., "Analysis of the Shimmy Phenomenon," *Proceedings of the Institution of Mechanical Engineers, Part G (Journal of Aerospace Engineering)*, Vol. 180, No. 10, 1965–1966, pp. 251–268.

[19] Doedel, E. J., "Notes on Numerical Analysis of Nonlinear Equations," *Numerical Continuation Methods for Dynamical Systems: Path Following and Boundary Value Problems*, edited by B. Krauskopf, H.

M. Osinga, and J. Galán-Vioque, Springer–Verlag, Berlin/New York/Heidelberg, 2007, pp. 1–49.

[20] Tanner, J. A., Daugherty, R. H., and Smith. H. C., "Mechanical Properties of Radial-Ply Aircraft Tires," *SAE transactions*, Vol. 114, No. 1, 2005.

[21] Thota, P., Krauskopf, B., and Lowenberg, M., "Shimmy in a Nonlinear Model of an Aircraft Nose Landing Gear with Nonzero Rake Angle," Institute of Problems of Mechanical Engineering Paper 54, 2008.

[22] Doedel, E. J., Champneys, A. R., Fairgrieve, T., Kuznetsov, Yu., Sandstede, B., and Wang, X., "AUTO 97: Continuation and Bifurcation Software for Ordinary Differential Equations," Computational Mathematics and Visualization Lab., Canada, May 2001.